2D Hexagonal Yttrium Doped SnO2 Nanoplatelets for Photocatalytic Degradation

S Vallimeena (valliabhi09@gmail.com)
B Helina

Research Article

Keywords: SnO2: Y, 2D hexagonal Nanoplatelets, Photocatalytic degradation

Posted Date: April 19th, 2022

DOI: https://doi.org/10.21203/rs.3.rs-1557162/v1

Abstract

In this work, two-dimensional hexagonal nanoplatelets were analyzed through a simple morphological and structural evolutions. XRD analysis of SnO_2 and Y doped SnO_2 has revealed a tetragonal structure and photoluminescence spectra exhibited a visible emission broadband peak around 464 nm and 528 nm. SnO_2: Y (7 wt.%) photoluminescence spectra confirm the higher charge separation and which impede the electron-hole recombination. It has been shown that hexagonal SnO_2:Y (7 wt.%) nanoplatelets perform better in photocatalytic degradation than conventional spherical nanoparticles. EIS measurements were performed to investigate the charge carrier movement of both undoped and Y doped SnO_2 NPs. Our study is the first to illustrate the two-dimensional morphology of SnO_2:Y (7 wt.%) hexagonal nanoplatelets and their application integration of photocatalytic materials.

1. Introduction

Morphology control is an important strategy for the development of functional nanomaterials such as promising transition metal oxide. Recently several techniques have been offered for waste water toxin elimination. By using photocatalytic treatment for removing organic pollutants from effluent is significant to prevent the demolition of ecologies [1]. Semiconductor photocatalysts have been broadly utilized for environmentally friendly issues like hazardous effluent remedies and energy troubles using plenteous solar light, with low cost, minimal toxicity, recyclable, as well as the capability for enhancing multi-step electron transport movements [2].

Recently the efforts have made to develop semiconductor materials having specific size, surface area, morphology and optical, electrical and catalytic features has gained attentiveness in the zones of conservation, biosystems and energy tenders [3]. Photocatalysts (PCs) based on tin oxide (SnO_2) are a simple and cost-effective method for destroying and eliminating the organic contaminants [4]. The yttrium ion is well suited for incorporation into SnO_2, since it has a comparable crystalline size as Sn^{4+}, resulting in high dispersion and enhanced electron-hole pair separation [5]. Controlling the morphology of SnO_2 is a critical technique for fine-tuning and optimizing the material's performance in photocatalytic applications. The different SnO_2 morphologies, i.e., 0D nanocubes [6] 1D nanotubes [7], nanobelts by thermal evaporation [8], 2D nanosheets [9] and 2D nanoplatelets (NPLs) [10,11]. 2D NPLs and nanosheets exhibit novel chemical and physical features, including anisotropically quantum-confined photocarriers, a unified exposed crystal facet, and a specified atomic arrangement on the surface. The applications of reported 2D nanostructure especially for sensing properties of SnO_2 NPLs [10], porous SnO_2 NPLs as Photoelectrodes and Gas Sensors [12] and 2D SnO_2 Nanosheets as an excellent sensing performance to Ethylene Glycol [9].

In this work, we report the first 2D hexagonal NPLs through a simple co-precipitation synthetic route at a room temperature. There are several methods for synthesis of NPLs such as hydrothermal [12] and thermal evaporation. Additionally, the produced 2D Y doped SnO_2 hexagonal NPLs act as an effective photocatalyst when illuminated with visible light. Our work not only demonstrates an efficient method for obtaining high-quality NPLs, but also paves the way for future investigations of morphologically controlled materials with increased performance for a broad range of applications.

2. Experimental Techniques

2.1 Materials

Tin chloride, Centyl trimethyl ammonium bromide (CTAB), Yttrium (III) acetate and ammonia solution supplied by Sigma Aldrich were used to synthesize SnO_2 and Y doped SnO_2. The chemicals employed for this work were not exposed to any other purification process. Double distilled water and ethanol is utilized as a solvent in the 2:1 for sample synthesis.

2.2 Synthesis of SnO_2 and Y doped SnO_2

10 gm of Tin chloride was dissolved in 90 ml of distilled water and ethanol, then allowed for stirring. The aqueous solution of CTAB was added for enhancing self-aggregation of nanoparticles. For precipitating ammonia solution was added drop by drop. The attained precipitate was cleansed with distilled water and ethanol to detach the remained impurities. The Y doped SnO_2 was synthesized by adding yttrium (III) acetate hydrate to the above stock solution.

3. Characterization

The morphology of the synthesized samples was probed with the Scanning electron microscope (SEM) (CAREL ZEISS, EVO 18). The structural analyses of the prepared samples were examined by XRD with the Bragg angles $10^\circ \leq 2\theta \leq 80^\circ$ through Cu target ($K\alpha$ = 1.5406 Å). Fourier Transmission Infrared Spectrometer (FTIR-7600 Lambda Intelligent) was used to inspect vibrational studies. The absorption spectrum was investigated through the UV–Vis–NIR spectrophotometer (Lambda 35 model). The photoluminescence spectra were studied by using Spectroflurophotometer (Shimadzu RF-5301) with an excitation wavelength of 330 nm. Versastat MC-Metex was used to analyse the Electrochemical impedance spectroscopy (EIS) measurements.

3.1 Evaluation of Photocatalytic Activities

The photocatalytic activity of the synthesized samples was evaluated for degrading MB dye mixture. 10 mg of SnO_2 and Y doped SnO_2 were mixed in 100 mL of MB dye mixture. Visible light radiation was utilized as a light source. The dye mixture was sustained in dark for 30 mins for confirming adsorption-desorption steadiness. The effluent pH was 7. By utilizing a spectrophotometer (Perkin spectrophotometer Elmer LAMBDA-35), the apparent absorption intensity of the effluent including the irradiation period was also examined. The degradation efficacy (%) is reckoned by the consequent formulation.

$$\text{Degradation Efficiency} = \frac{\left(C_0 - C\right)}{C_0} \times 100\% \quad (1)$$

Where C_0 and C denotes the dye mixture concentrations of the effluent at initial (t = 0) and at time t respectively.

4. Results And Discussions

4.1 Morphological and Structural Analysis

The surface morphology of SnO_2, and Yttrium (Y) doped SnO_2 NPs (3,5 and 7 wt.%) are analyzed by SEM is shown in Fig. 1(a). Undoped SnO_2 reveals the spherical NPs and agglomerations of spherical NPs are augmented with increasing the dopant content (3 and .5 wt.%) shown in Fig. 1(b, c). 7 wt.% Y doped SnO_2 exhibits 2D platelet shape (Fig. 1d) and its surface has quite soft, with no existence of any secondary nanostructures. The doping content of Y affects the host SnO_2 and the obtained nanoplatelets are in the nanoscale region.

On the other hand, as a result of the high surface energy, the initial crystal grains combine in an orderly fashion to form layered SnO_2 by directed attachment growth. To limit the overall surface area, it may be argued that an emphasis should be placed on orderly attachment development in the same horizontal plane [13]. The 7 wt.% Y doped SnO_2 nanoplatelets are reinforced by the addition of ligands that inhibit growth in other directions. Here, nanoplatelets are formed initially as a few seeds that grow longer with continued slow addition of precursors. At 500°C, the production of two-dimensional SnO_2 nanoplatelets may be attributed to the template effect of their precursor [11].

The effective growth of SnO_2, and Y doped SnO_2 NPs is validated over EDAX spectrum demonstrated in Fig. 2a, b and c. The nanoparticles mostly comprise of Sn, O and Y. A described elemental composition and weight % are presented in inset of Fig. 2. The amount of Y^{3+} ion showed on EDAX spectrum, which is reliable with the amount included in the synthesis step.

The XRD pattern of SnO_2, and Y doped SnO_2 hexagonal NPLs are displayed in Fig. 3. It exhibits a distinct diffraction peaks, and which is indexed as the tetragonal structure of SnO_2 with JCPDS card no. 71–0467. The positions of the diffraction peaks (2θ = 26.6°, 33.9°, 37.9°, 51.8°, 54.9°, 57.7°, 61.9°, and 64.9°) matched with the crystal plane ((110), (101), (200), (211), (220), (310), (112), and (301), respectively) [14]. The absence of impurities indicates that yttrium element doping had no effect on the crystal structures. By compared with XRD of pure SnO_2, the diffraction peaks of Y doped SnO_2 lattice planes shift to the low-angle due to the replacement of Y^{3+} ions (radius 89 pm) with Sn^{4+} (radius 69 pm) and which validates that the Y^{3+} ions have been doped into the SnO_2 lattices. The crystallite size is determined by Scherrer's equation, and it is found to be 17 nm for SnO_2, and 18.2, 20, and 22 nm for 3,5 and 7 wt.% Y doped SnO_2 nanoparticles.

4.2 Vibrational Analysis

FT-IR is an effective device for identifying the functional groups and the kinds of chemical bonds. Figure 4 shows the FTIR spectra of SnO_2, and Yttrium doped SnO_2. The absorption band at 3437 – 3434 cm^{-1} and 1637 – 1627 cm^{-1} for SnO_2, and Yttrium doped SnO_2 is known as stretching and bending mode of OH groups related to the adsorbed/re-adsorbed water over the SnO_2 surface. The peak observed at 2941 – 2935 and 2853 cm^{-1} indicates the antisymmetric (d^-) and symmetric (d^+) CH_2 stretches of hydrocarbon chains of the CTAB [15]. The band detected at 1395 – 1383 cm^{-1} was due to the C-H deformation vibration. The FT-IR spectra bands at 1106 – 1044 cm^{-1} is ascribed to C–O–C vibration mode. The strong apex observed at 567 – 557 and 641 – 621 cm^{-1} accord to the metal–oxygen for anti-symmetric O–Sn–O and Sn–O lattice stretching wave modes [1]. When dopant concentration is increased the peak observed at 567 cm^{-1} gets decreased and at higher concentration it is diminished. It validates incorporation of dopant ion into the SnO_2. In addition, the

absorption processes were not noticed further, confirming the coherent dispersion of dopant ions and indicate the precision of the synthesized samples. Furthermore, the shifts to lower wavenumber for Y doped SnO_2 may be interpreted via the dissimilarity in the bond length or strength of Sn^{4+} and O_2^- bond [16]. The strong bands associated with OH groups in the synthesized samples designates the SnO_2, and Y doped SnO_2 may accomplish higher photocatalytic activity and it inhibits the recombining of electron–hole pairs [17].

4.3 Optical Studies

Figure 5(a) shows the UV-DRS spectra of SnO_2, and Y doped SnO_2 nanoparticles. Undoped SnO_2 exhibits a strong peak at ~ 289 nm, while Yttrium (3wt.%, 5 wt.% and 7 wt.%) doped SnO_2 reveals the absorption peak at ~ 292, 295 and 305 nm respectively. As compared to the Undoped SnO_2 the absorption edges of Yttrium doped SnO_2 is red shifted increasingly. Whereas the dopants and defects are existed, further extrinsic electronic points may well reside in the Energy gap (Eg) of the SnO_2. Furthermore, the optical property is enriched henceforth the Y doped SnO_2 comprises into the visible light region because of the incorporation of Y dopants into SnO_2 lattice. Additionally, the red shifted optical absorption superiority of Y doped SnO_2 to the lesser energy level.

The absorption is proportional to reflectance, then the absorption coefficient (α) is replaced by F(R). The band gap is calculated by Tau's plot. The obtained band gap is 3.77, 3.67, 3.58, and 3.46 eV for 0%, 3wt.%,5wt.% and 7 wt.% doped SnO_2 correspondingly as shown in Fig. 5(b) and it is found that the E_g of the Y doped SnO_2 sample decreases. The Eg of SnO_2 NPs is found to be higher than the bulk SnO_2 (3.6 eV) due to the quantum confinement and their absorption edges showed a red shift with an increasing in the dopant concentration because of following causes; SnO_2 is a degenerate semiconductor, and its Fermi level remains within the conduction band (CB). Since E_g is correlated to the excitation of the electrons from the valance band (VB) to Fermi level [18]. It suggests that the Fermi level moving towards the lowest of CB of the semiconductor owing to the reduction in the carrier concentration precedes narrowing the E_g through the replacement by Y^{3+} ions on several Sn^{4+} ions in the lattice. Moreover, the decrease in energy E_g may be due to the spin-exchange interactions. The shift of E_g by Y ion doping may be ascribed to the Moss-Burstein (MB) effect.

Typically, the photoluminescence (PL) emission spectra are utilized for investigating electron-hole evolutions over semiconductor surfaces and therefore resolve the surface defect in the samples. The PL emission spectra of SnO_2 and Y doped SnO_2 nanoparticles are revealed in Fig. 5(c) under an excitation wavelength of ~ 320 nm. The blue and green emission peak is observed at 464 nm and 528 nm in all synthesized samples. The blue emission peak exhibits the shallower trapped states within energy gap, enormous oxygen vacancies and surface defects in the prepared samples [19]. At 433 nm, the band is ascribed to defect centers inside the energy gap and in-plane oxygen vacancies [20]. The higher oxygen vacancies are the most prevalent defect in nanocrystalline metallic oxides that serve as luminous centers. SnO_2 emits light at 540 nm, which is caused by structural defects such as Sn interstitials [21]. The PL spectra of Y doping results suggest that the decrease in the E_g of SnO_2 and endorse photo-response ability, creating numerous active positions inside the SnO_2 among VB and CB by Y^{3+} ion exchange. This shows that the larger separation of the photoexcited electron–hole recombination has weak peak intensity, which grades in the realization of reactive surface interiors instigated via additional Y^{3+} for enhancing photodegradation efficiency.

4.4 Impedance measurement

Figure 5d shows the Nyquist plot of SnO_2 and Y doped SnO_2 nanoparticles. A semicircle and a straight line are shown in these figures (low-frequency region). The radius of the arc denotes the higher frequency zone, and the value of the charge transfer resistance corresponds to this region (Rct). The semicircle radius of the Nyquist cross-section is proportional to the interface charge migration, which is dependent on the prepared sample's charge separation efficiency. The 7 wt. % Y doped SnO_2 exhibits a smaller semicircle in the higher frequency zone, indicating that the doped electrode has a reduced charge transfer resistance [22]. The charge transfer resistance (Rct) of SnO_2, 5% wt. % Y doped SnO_2 nanoparticles is 46816, 37156, and 29177 Ohm, respectively. These values are lower than those previously reported for La doped SnO_2 [23]. In comparison to SnO_2, the arc radius of 7 wt.% Y doped SnO_2 nanoparticles is lower, which results in a low charge transfer resistance. Because the presence of yttrium in SnO_2 enhances charge carrier movement.

4.5 Photocatalytic Degradation

The SnO_2 and SnO_2: Y NPs were utilized as photocatalyst for degradation of MB dye under visible light source. Figure 6 (a–d) shows the absorption spectrum of an aqueous MB dye solution in the presence of photocatalysts. As seen in Fig. 6, it shows the characteristic absorption peak intensity of MB (664 nm) that is effectively lowered with illumination duration due to the degradation process. For SnO_2:Y (7 wt. %) hexagonal NPLs, the distinctive MB absorption peak reduced after 120 minutes of irradiation. This indicates that hexagonal SnO_2:Y (7 wt.%) NPLs have higher photocatalytic activity than other samples. Additionally, when Y^{3+} is added to SnO_2, the degradation efficiency is increased further in comparison to the dye molecules evaluated. The presence of a large number of Y^{3+} ions inside the structure creates an oxygen vacancy, which prevents electron and hole recombination, hence increasing photocatalytic efficiency.

4.5.1 Photocatalytic Mechanism

Electrons in the valence band (VB) are stimulated into the conduction band when they absorb enough photon energy to generate holes (CB). In CB, electrons produced during photosynthesis may interact with neighboring O_2 to generate a superoxide anion (O^-_2.). Similarly, the holes react with hydrogen molecules in H_2O to form hydroxyl radicals (OH.). O^-_2. and OH. participate in the decomposition of dye molecules. These O_2. and OH. can efficiently react with dye molecules and create carbon dioxide and water [24]. However, the wide bandgap of SnO_2 and easy recombination of charge carriers determines the photocatalytic efficiency of SnO_2. Therefore, SnO_2 shows a relatively low efficiency. Scheme.1 displays the Photocatalytic mechanisms of prepared SnO_2: Y NPLs. Yttrium doped SnO_2 photocatalyst alters the rapidity of photodegradation and systematic path of waste products. The improvement in photocatalytic activity was primarily due to the creation of oxygen vacancies and the improvement in effective electron mobility. When the Sn^{4+} ions are replaced with Y^{3+}, an oxygen vacancy will occur in SnO_2. Oxygen vacancy on surfaces can increase O_2 adsorption and function as a center for capturing photo-induced electrons through photocatalytic reaction activities. Oxygen vacancies delay the recombination of electron-hole pairs and also enhanced photocatalytic processes [7].

Furthermore, nano platelet 2D structure with lower bandgap energy of SnO_2: Y (7 wt.%) has higher photocatalytic degradation compared with spherical morphology. Since 2D SnO_2: Y (7 wt.%) NPLs possess a high percentage of surface atoms, superior free-charge mobilities, and a short distance to surface catalytic sites, it is shown that the 2D morphology can greatly promote their performances in photocatalytic reactions [25, 26]. Such a drastically improved photocatalytic performance of SnO_2:Y (7 wt.%) NPLs was likely due to the anisotropically confined charge carries and their in-plane long diffusion length for the NPLs as compared to undoped and Y doped SnO_2 spherical NPs. The surface morphology and bandgap have a significant effect on the photocatalytic efficiency of SnO_2: Y (7 wt.%) semiconductors.

The rate of degradation of the dye solution is calculated based on pseudo-first-order kinetics and tested using the Langmuir-Hinshelwood model and given by the relation $k = \ln (C_0 / C) / t$ where C_0 and C represent the concentration of the dye solution at initial (t_0) and time t and k times are the so-called first-order velocity constant [17]. The relationship between the natural logarithm of C_0/C and irradiation time (t) for SnO_2 and SnO_2: Y is shown in Fig. 7 (a, b). The evaluated degradation efficiency (%) of SnO_2, the rate constant (k) and regression coefficient (R^2) are presented in Table 1. The high R^2 value obtained, indicates that the prepared catalyst has good first-stage pseudo-model kinetics. The correlation value is almost 1 showing the best adsorption rate [27]. These outcomes validated that SnO_2:Y (7 wt.%) was successfully synthesized by Y as a dopant which has a better photocatalytic performance than other samples. Various reported photocatalytic activity of doped SnO_2 photocatalysts are listed in Table 2.

Table 1
Degradation efficiency (%), Rate constant (k) and Regression coefficient (R^2) of the undoped and Y doped SnO_2 photocatalysts

Sample	**MB dye (120 min.)**		
	Efficiency (%)	**R^2**	**K**
SnO_2	66	0.9522	0.00931
SnO_2: Y (3 wt. %)	**68**	0.97118	0.00955
SnO_2: Zn (5 wt. %)	70	0.9772	0.01076
SnO_2: Zn (7 wt. %)	82	0.9873	0.01320

Table 2
Several reported photocatalytic activities of doped SnO_2 photocatalysts

Photocatalyst	Synthesis Method	Morphology	Light source	Dye	Quantity Used	Efficiency (%)	Ref.
SnO_2: Y	Coprecipitation	Hexagonal nanoplatelets	Visible	Methylene blue	10 mg	82% (120 min)	This study
SnO_2: Y	Hydrothermal	Spherical	Visible	Methylene blue	10 mg	92.34% (180 min)	[1]
SnO_2 : V	Coprecipitation	Spherical shape	UV light	RhB	50 mg	95% (150 min)	[28]
SnO_2 : Eu	Hydrothermal	Nanorod	UV	RhB	40 mg	90% (70 min)	[29]
SnO_2 : Ce SnO_2 : Nd SnO_2 : La	Sol–gel	Spherical shape	UV	Phenol	65 mg	86%, 57% , 100% (30 min)	[30]
$Sn_{0.95}Cu_{0.03}Y_{0.02}O_2$	Coprecipitation	Spherical shape	Solar light	Cango red, RhB	0.1 gm	78%, 70%, (90 min)	[24]

4.6 Conclusion

The enhanced photocatalytic activity of SnO_2:Y (7 wt.%) hexagonal nanoplatelets may be attributed to increased optical absorption, effective charge separation of photogenerated charge carriers, and reduced electron-hole recombination. 7 wt.% doped SnO_2 decreased the bandgap and the replacement of $Y^{3+}$with Sn^{4+} ions enhances the oxygen vacancy on surfaces which can increase O_2 adsorption and function as a center for capturing photo-induced electrons through photocatalytic reaction activities. The presence of defects and mechanism of charge carrier recombination is confirmed by photoluminescence spectra. Moreover, the electrochemical performance of the SnO_2: Y (7 wt.%) NPLs confirms the higher charge separation efficiency. Our demonstrated simple co-precipitation methodology for the synthesis of SnO_2:Y (7 wt.%) 2D hexagonal nanoplatelets have environmental applications in the degradation of MB dye solution.

Declarations

Acknowledgement

The Authors would like to thank Manonmaniam Sundaranar University, Tamilnadu, for undertaking the pre-doctoral degree (Register No. 18221282132007). We also thank the Department of physics, St. Xavier's College (Autonomous), Palayamkottai for providing facilities for the fulfillment of the research work.

References

1. Ali Baig, A. B., Rathinam, V., & Palaninathan, J. Photodegradation activity of yttrium-doped SnO2 nanoparticles against methylene blue dye and antibacterial effects. Applied Water Science, 10(2), 1-13 (2020).
2. Xu, C., Anusuyadevi, P. R., Aymonier, C., Luque, R., & Marre, S. Nanostructured materials for photocatalysis. *Chemical Society Reviews*, *48*(14), 3868-3902 (2019).
3. Jayapandi, S., Premkumar, S., Lakshmi, D., Packiyaraj, P., Sivaraj, P., & Anitha, K. Reinforced photocatalytic reduction of SnO2 nanoparticle by La incorporation for efficient photodegradation under visible light irradiation. Journal of Materials Science: Materials in Electronics, 30(9), 8479-8492 (2019).
4. Vignesh, S., Suganthi, S., Sundar, J. K., Raj, V., & Devi, P. R. I. Highly efficient visible light photocatalytic and antibacterial performance of PVP capped Cd: Ag: ZnO photocatalyst nanocomposites. Applied Surface Science, 479, 914-929 (2019).
5. Liu, J., Yang, R., & Li, S. Synthesis and photocatalytic activity of TiO_2/V_2O_5 composite catalyst doped with rare earth ions. Journal of Rare Earths, 25(2), 173-178 (2007).
6. Khalid, M.U., Khan, S.R. & Jamil, S. Morphologically Controlled Synthesis of Cubes like Tin Oxide Nanoparticles and Study of its Application as Photocatalyst for Congo Red Degradation and as Fuel Additive. J Inorg. Organomet. Polym 28, 168–176 (2018).
7. Sadeghzadeh-Attar, A. J. S. E. M. Efficient photocatalytic degradation of methylene blue dye by SnO2 nanotubes synthesized at different calcination temperatures. Solar Energy Materials and Solar Cells, 183, 16-24 (2018).
8. Li, X., Liu, Y., Li, S., Huang, J., Wu, Y., & Yu, D. The sensing properties of single Y-doped SnO 2 nanobelt device to acetone. Nanoscale research letters, 11(1), 1-8 (2016).
9. Wan, W., Li, Y., Ren, X., Zhao, Y., Gao, F., & Zhao, H. 2D SnO2 nanosheets: synthesis, characterization, structures, and excellent sensing performance to ethylene glycol. Nanomaterials, 8(2), 112 (2018).
10. Li, K. M., Li, Y. J., Lu, M. Y., Kuo, C. I., & Chen, L. J. Direct Conversion of Single-Layer SnO Nanoplates to Multi-Layer SnO2 Nanoplates with Enhanced Ethanol Sensing Properties. Advanced Functional Materials, 19(15), 2453-2456 (2009).
11. Wang, A. R., Xiao, H. Controllable preparation of SnO_2 nanoplates and nanoparticles via hydrothermal oxidation of SnS_2 nanoplates. Materials Letters, 63(13-14), 1221-1223 (2009).
12. Zhang, Y. Z., Pang, H., Sun, Y., Lai, W. Y., Wei, A., & Huang, W. Porous tin oxide nanoplatelets as excellent-efficiency photoelectrodes and gas sensors. Int. J. Electrochem. Sci, 8, 3371-3378 (2013).
13. Wan, W., Li, Y., Ren, X., Zhao, Y., Gao, F., & Zhao, H. 2D SnO2 nanosheets: synthesis, characterization, structures, and excellent sensing performance to ethylene glycol. Nanomaterials, 8(2), 112 (2018).
14. Li, X., Liu, Y., Li, S., Huang, J., Wu, Y., & Yu, DThe sensing properties of single Y-doped SnO_2 nanobelt device to acetone. Nanoscale research letters, 11(1), 1-8 (2016).

15. Campbell, R. A., Parker, S. R., Day, J. P., & Bain, C. D. External reflection FTIR spectroscopy of the cationic surfactant hexadecyltrimethylammonium bromide (CTAB) on an overflowing cylinder. Langmuir, 20(20), 8740-8753 (2004).
16. Phukan, A., Bhattacharjee, R. P., & Dutta, D. K. Stabilization of SnO2 nanoparticles into the nanopores of modified Montmorillonite and their antibacterial activity. Advanced Powder Technology, 28(1), 139-145 (2017).
17. Suganthi, N., & Pushpanathan, K. Photocatalytic degradation and antimicrobial activity of transition metal doped mesoporous ZnS nanoparticles. International journal of environmental science and technology, 16(7), 3375-3388 (2019).
18. Babar, A. R., Shinde, S. S., Moholkar, A. V., Bhosale, C. H., Kim, J. H., & Rajpure, K. Y. Sensing properties of sprayed antimony doped tin oxide thin films: solution molarity. Journal of Alloys and Compounds, 509(6), 3108-3115 (2011).
19. Kumar, V., Yadav, S. K., Gupta, A., Dwivedi, B., Kumar, A., Singh, P., & Deori, K. Facile synthesis of Ce–doped SnO_2 nanoparticles: a promising photocatalyst for hydrogen evolution and dyes degradation. Chemistry Select, 4(13), 3722-3729 (2019).
20. Luo, S., Chu, P. K., Liu, W., Zhang, M., & Lin, C. Origin of low-temperature photoluminescence from Sn O 2 nanowires fabricated by thermal evaporation and annealed in different ambients. Applied Physics Letters, 88(18), 183112 (2006).
21. Shajira, P. S., Bushiri, M. J., Nair, B. B., & Prabhu, V. G. Energy band structure investigation of blue and green light emitting Mg doped SnO2 nanostructures synthesized by combustion method. Journal of luminescence, 145, 425-429 (2014).
22. Suthakaran, S., Dhanapandian, S., Krishnakumar, N., & Ponpandian, N. Hydrothermal synthesis of surfactant assisted Zn doped SnO_2 nanoparticles with enhanced photocatalytic performance and energy storage performance. Journal of Physics and Chemistry of Solids, 141, 109407 (2020).
23. Jayapandi, S., Packiyaraj, P., Premkumar, S., Mayandi, J., & Anitha, K. Influence of pH in La-doped SnO_2 nanoparticles towards sensor applications. Ionics, 23(10), 2909-2917 (2017).
24. Saad Mabrouk Yakout, Engineering of visible light photocatalytic activity in SnO2 nanoparticles: Cu2+-integrated Li+, Y3+ or Zr4+ dopants, Optical Materials 116 (2021) 111077.
25. Voiry, D., Shin, H. S., Loh, K. P., & Chhowalla, M. Low-dimensional catalysts for hydrogen evolution and CO2 reduction. Nature Reviews Chemistry, 2(1), 1-17 (2018).
26. Su, T., Shao, Q., Qin, Z., Guo, Z., & Wu, Z. Role of interfaces in two-dimensional photocatalyst for water splitting. Acs Catalysis, 8(3), 2253-2276 (2018).
27. Adeyemi, J. O., Elemike, E. E., & Onwudiwe, D. C. ZnO nanoparticles mediated by aqueous extracts of Dovyalis caffra fruits and the photocatalytic evaluations. Materials Research Express, 6(12), 125091 (2019).
28. Letifi, H., Litaiem, Y., Dridi, D., Ammar, S., & Chtourou, R. Enhanced photocatalytic activity of vanadium-doped SnO_2 nanoparticles in rhodamine B degradation. Advances in Condensed Matter Physics, 2157428 (2019).

29. Kaur, H., Bhatti, H. S., & Singh, K. Europium doping effect on 3D flower-like SnO nanostructures: morphological changes, photocatalytic performance and fluorescence detection of heavy metal ion contamination in drinking water. 9, 37450-37466 (2019).
30. Al-Hamdi, A. M., Sillanpää, M., & Dutta, J. Photocatalytic degradation of phenol in aqueous solution by rare earth-doped SnO_2 nanoparticles. Journal of Materials Science, 49(14), 5151-5159 (2014).

Scheme

Scheme 1 is available in the Supplementary Files section.

Figures

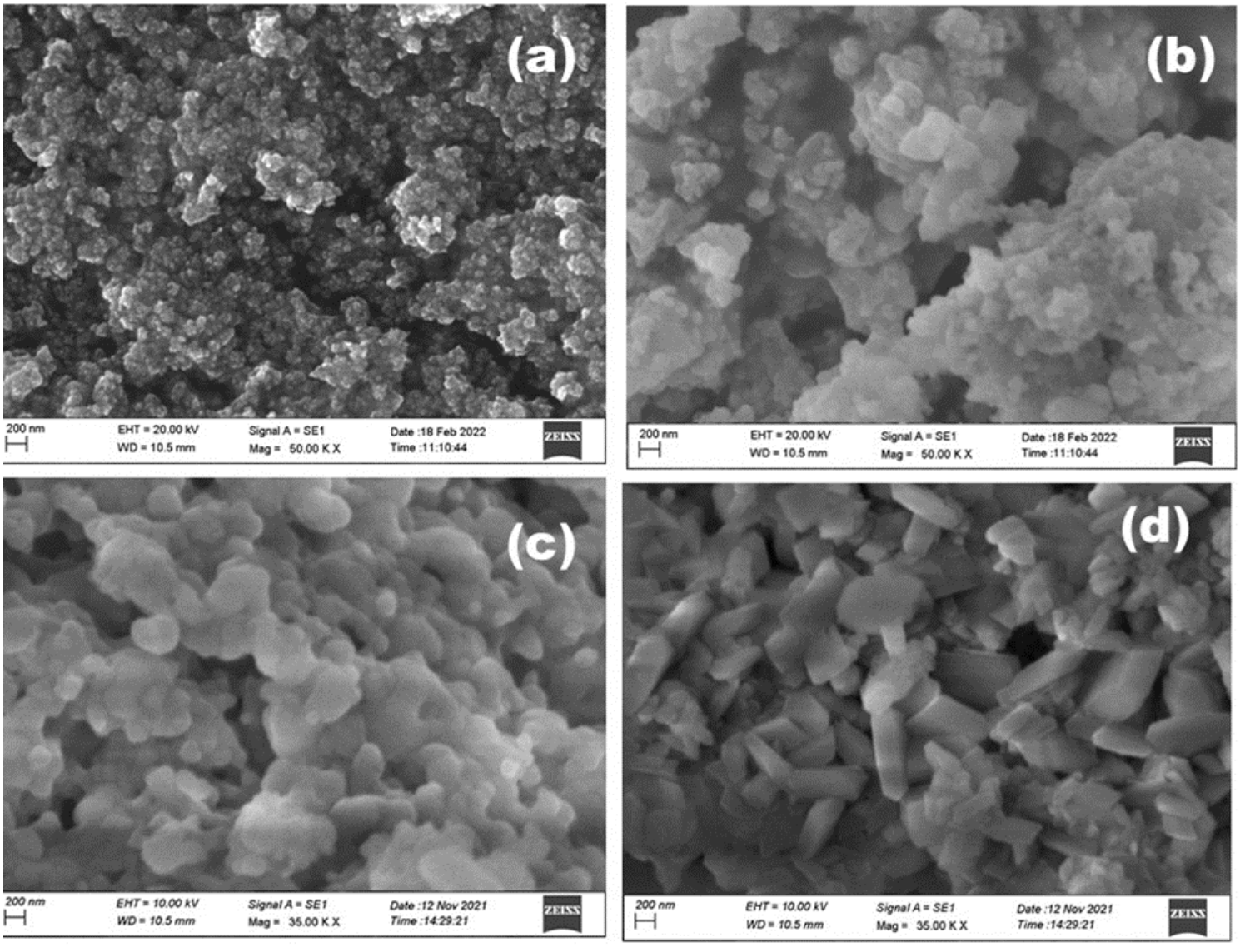

Figure 1

SEM images of (a) undoped, (b) 3 wt.%, (c) 5 wt.% and (d) 7 wt.% Y doped SnO_2

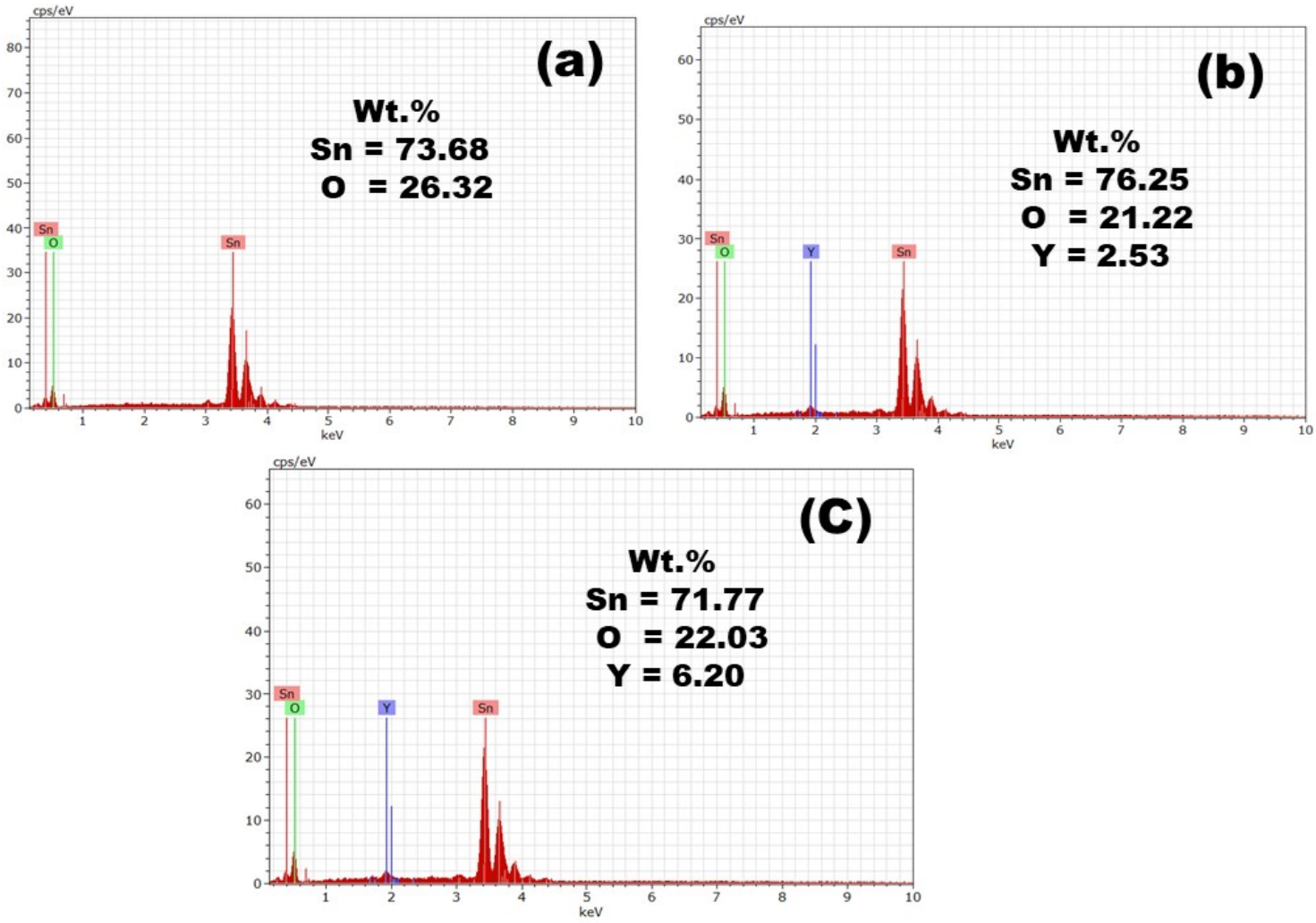

Figure 2

EDAX spectrum of (a) undoped (b) 3 wt.% and (c) 7 wt.% Y doped SnO_2

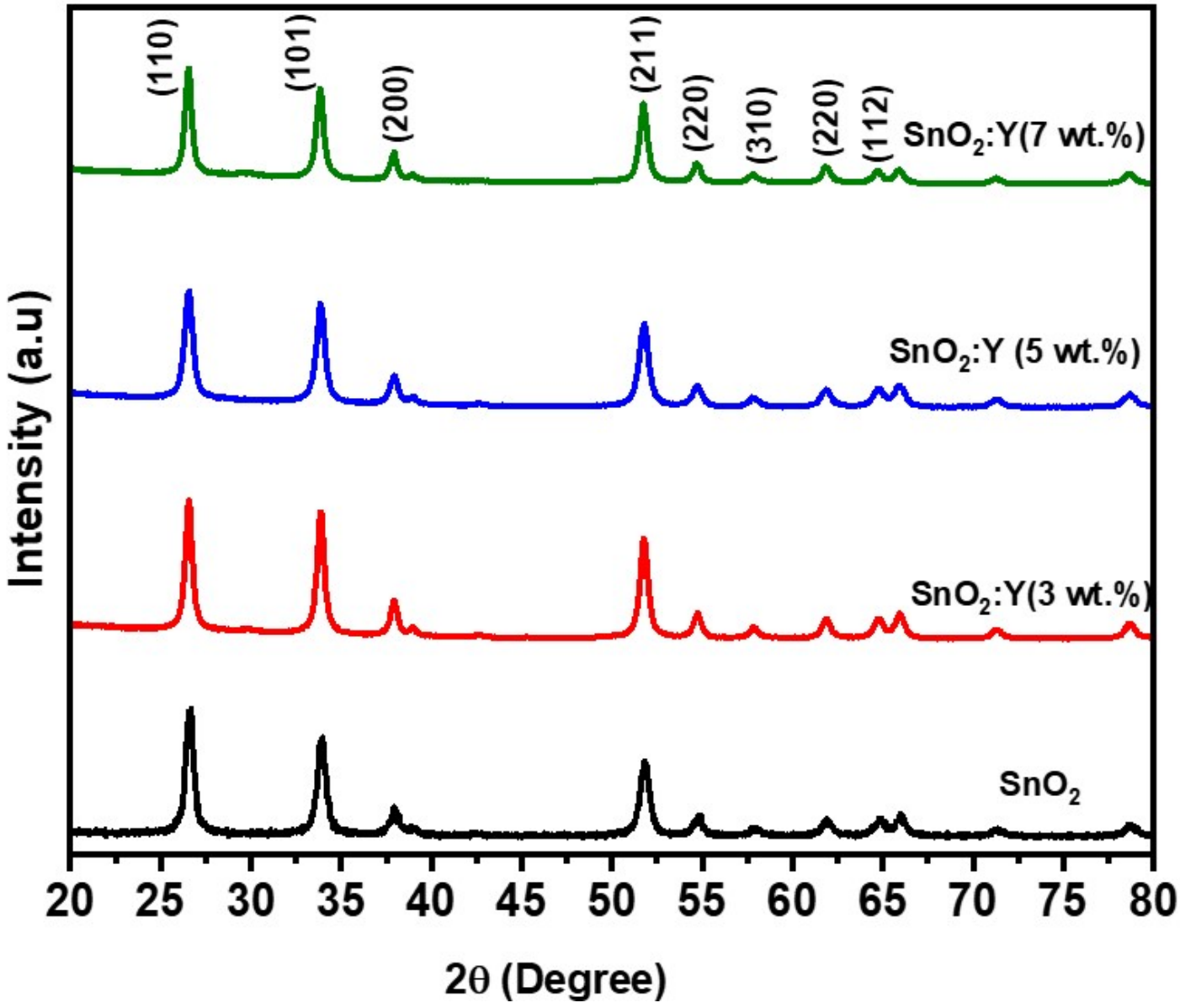

Figure 3

XRD spectra of (a) SnO_2 and Y doped SnO_2

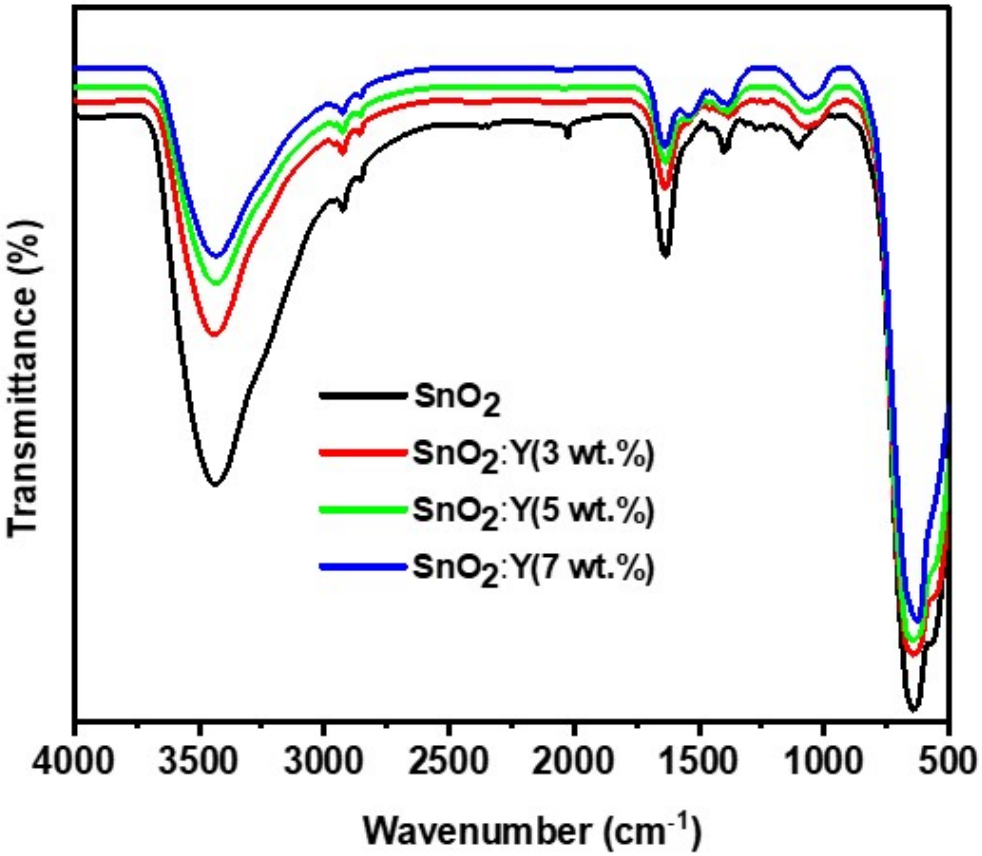

Figure 4

FTIR spectra of SnO_2 and Y doped SnO_2 nanoparticles

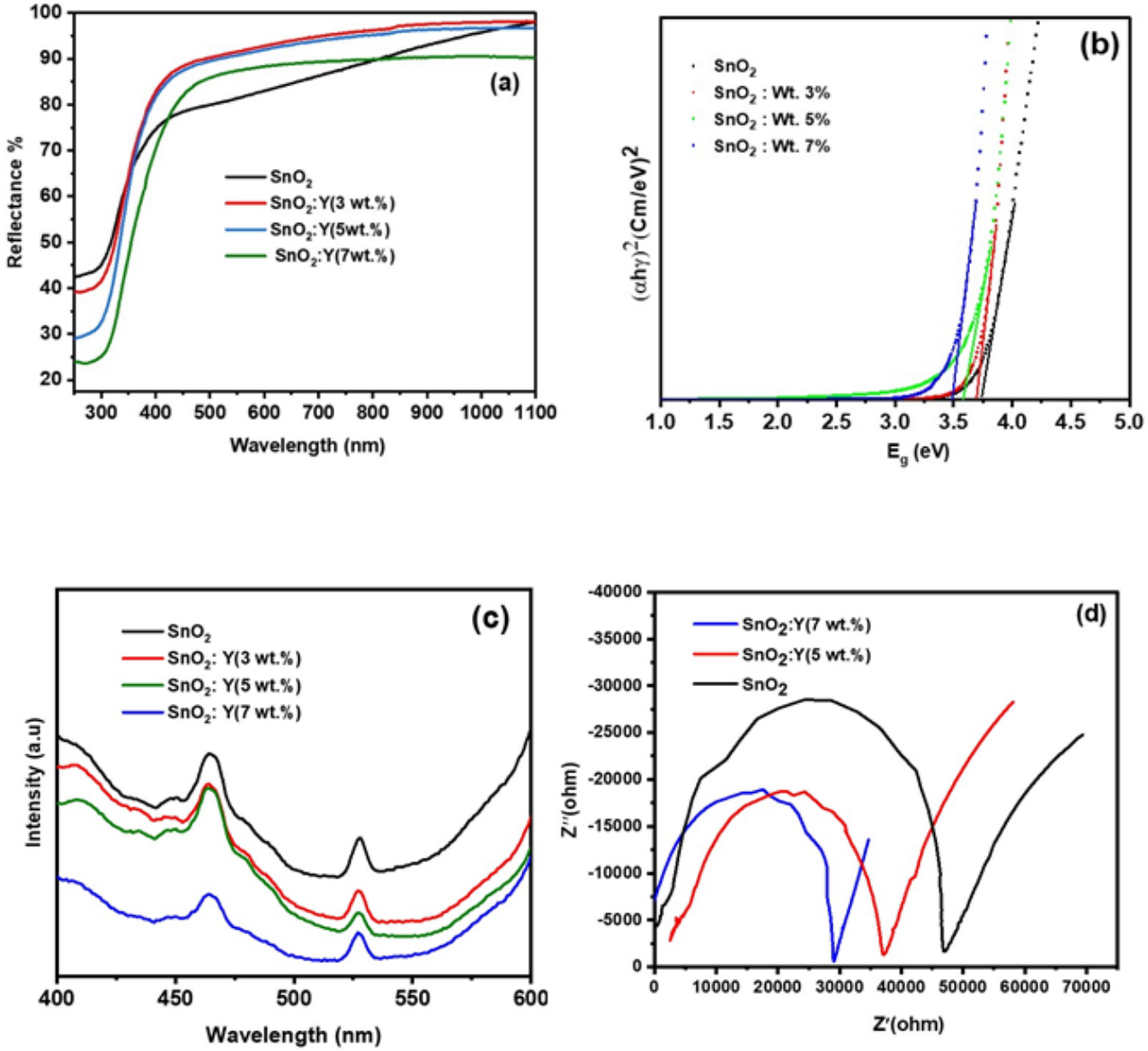

Figure 5

(a) UV-DRS spectra, (b) band gap calculation by Tau's plot, (c) Photoluminescence spectra and (d) EIS spectra of SnO_2 and Y doped SnO_2 nanoparticles

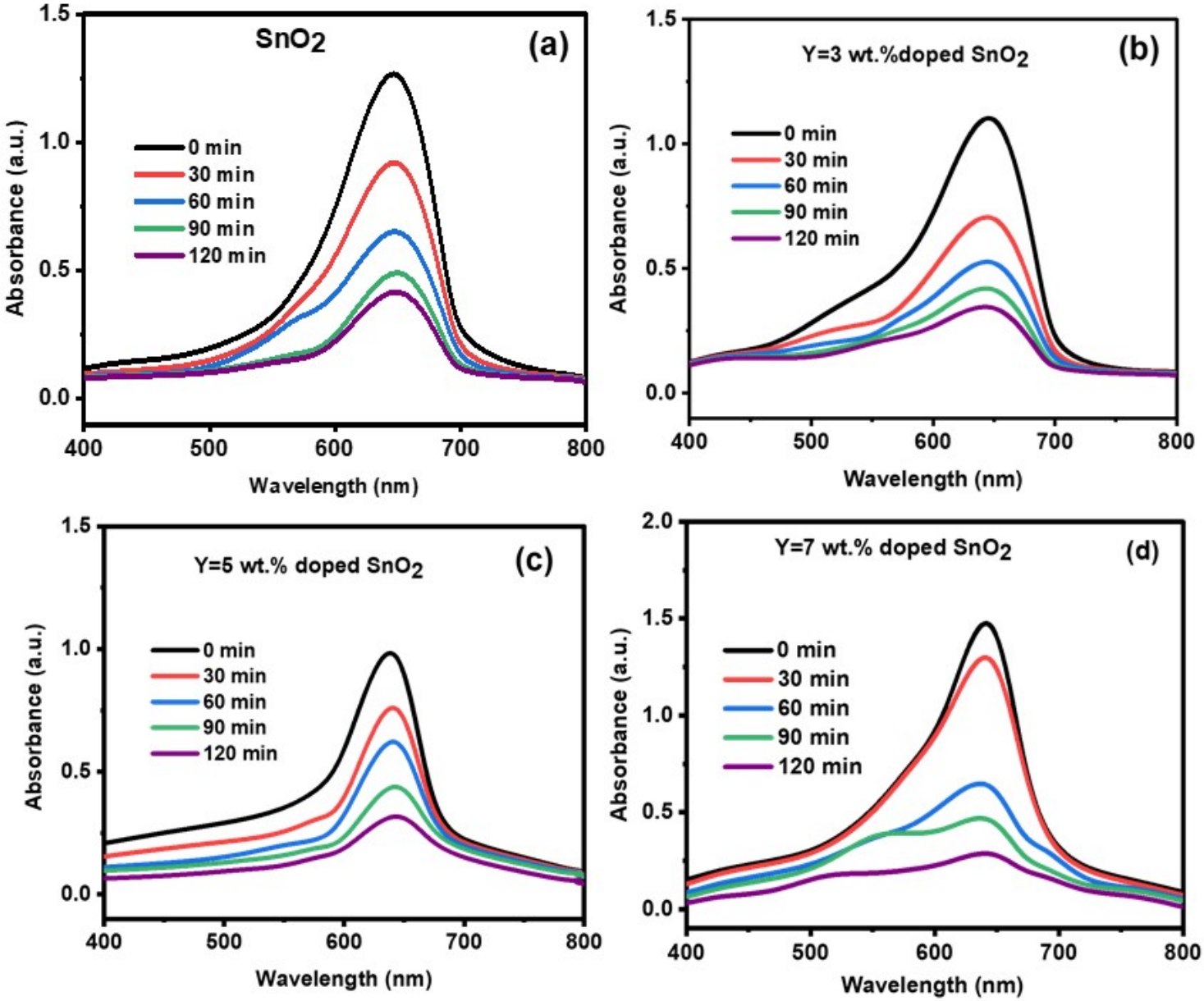

Figure 6

Absorbance spectra of MB dye in the presence of (a) undoped, (b) 3 wt.%, (c) 5 wt.% and (d) 7 wt.% Y doped SnO_2 nanoparticles

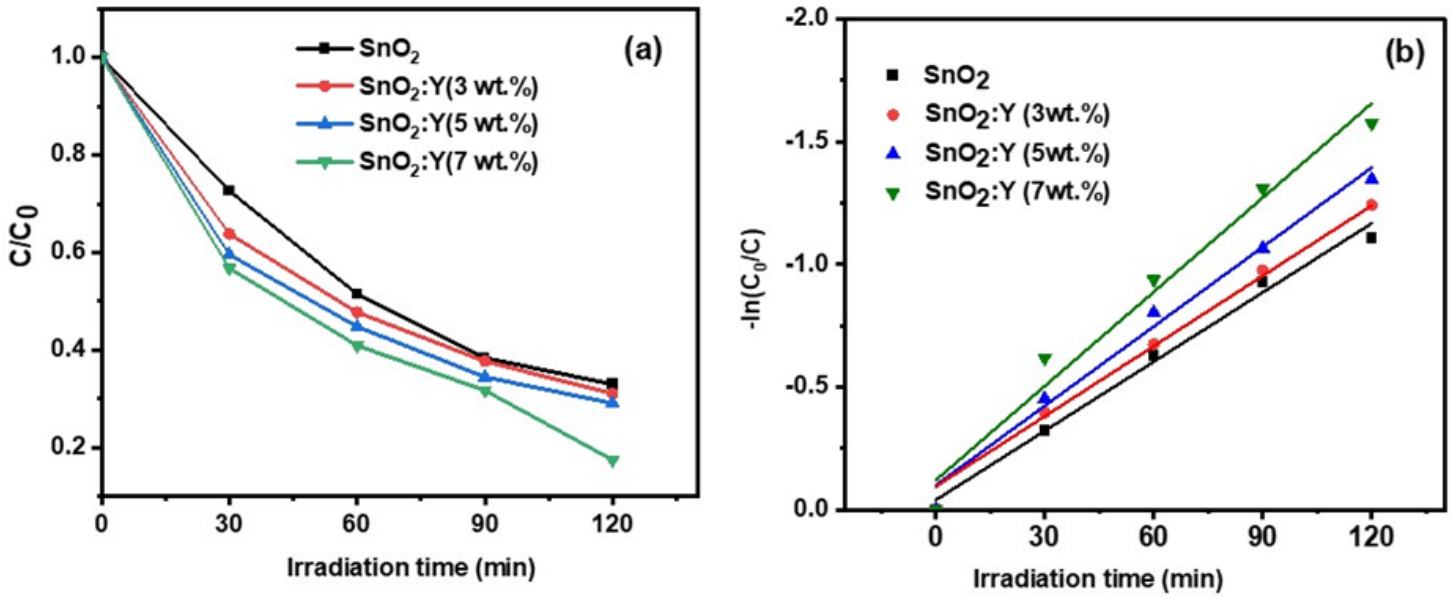

Figure 7

(a) Plots of (C/C_0) and (b) Plots of $-\ln(C_0/C)$ against irradiation time for undoped and Y doped SnO_2 nanoparticles

Supplementary Files

This is a list of supplementary files associated with this preprint. Click to download.

- Scheme.1.png